

Chemical abundance analysis of symbiotic giants – II. AE Ara, BX Mon, KX TrA, and CL Sco

Cezary Gałan^{1*}, Joanna Mikołajewska¹, and Kenneth H. Hinkle²

¹*N. Copernicus Astronomical Center, Bartycka 18, PL-00-716 Warsaw, Poland*

²*National Optical Astronomy Observatory, PO Box 26732, Tucson, AZ 85726, USA*

Accepted 2014 November 12. Received 2014 October 10

ABSTRACT

Knowledge of the elemental abundances of symbiotic giants is essential to address the role of chemical composition in the evolution of symbiotic binaries, to map their parent population, and to trace their mass transfer history. However, there are few symbiotic giants for which the photospheric abundances are fairly well determined. This is the second in a series of papers on chemical composition of symbiotic giants determined from high-resolution ($R \sim 50000$) near-IR spectra. Results are presented for the late-type giant star in the AE Ara, BX Mon, KX TrA, and CL Sco systems. Spectrum synthesis employing standard local thermal equilibrium (LTE) analysis and stellar atmosphere models were used to obtain photospheric abundances of CNO and elements around the iron peak (Sc, Ti, Fe, and Ni). Our analysis resulted in sub-solar metallicities in BX Mon, KX TrA, and CL Sco by $[\text{Fe}/\text{H}] \sim -0.3$ or -0.5 depending on the value of microturbulence. AE Ara shows metallicity closer to solar by ~ 0.2 dex. The enrichment in ^{14}N isotope found in all these objects indicates that the giants have experienced the first dredge-up. In the case of BX Mon first dredge-up is also confirmed by the low $^{12}\text{C}/^{13}\text{C}$ isotopic ratio of ~ 8 .

Key words: stars: abundances – stars: atmospheres – binaries: symbiotic – stars: individual: AE Ara, BX Mon, KX TrA, CL Sco – stars: late-type

1 INTRODUCTION

Symbiotic stars are long-period binary systems composed of two evolved and strongly interacting stars: a red giant donor and a hot luminous white dwarf companion (occasionally replaced by a neutron star) surrounded by an ionized nebula. Mass exchange between the binary system members is critical in defining their evolution. Mass-loss from the giant undergoes accretion to the compact object via wind and/or Roche lobe overflow (Podsiadlowski & Mohamed 2007, Mikołajewska 2012) resulting in the formation of an accretion disc and jet (Solf & Ulrich 1985, Tomov 2003, Angeloni et al. 2011). The hot companion had previously passed through a red giant stage. In the previous red giant stage mass was transferred from this star to the star that is currently a red giant. Abundance signatures tracing this mass transfer process have been measured in some red giant–white dwarf binary systems (Smith & Lambert 1988). In some cases the mass transfer process can result in symbiotic progenitors for supernovae Type Ia (SNe Ia). Symbiotic systems are believed responsible for between a few per cent to 30 per cent of SNe Ia events (Dilday et al. 2012, Mikołajewska 2012).

The complex structure with many types of interactions make symbiotic stars excellent laboratories for studying various aspects of red giant branch (RGB)/ asymptotic giant branch (AGB) bi-

nary evolution. Knowledge of the chemical composition in symbiotic giant's atmospheres can be used to track the mass exchange history as well as the population origin of the stellar material. However, reliable determinations of photospheric compositions exist for only a small number of objects, mostly G- or K-type giants, whereas the vast majority of symbiotic stars contain M-type giants. Prior to the current series of papers only four M giants in S-type symbiotic systems had been analysed in the literature: V2116 Oph (Hinkle et al. 2006), T CrB, RS Oph (Wallerstein et al. 2008), and CH Cyg (Schmidt et al. 2006). All of them had solar or nearly solar metallicities. The rarer symbiotic stars containing K-type giants are metal-poor with s-process elements overabundant (Smith et al. 1996, 1997; Pereira et al. 1998; Pereira & Roig 2009) whereas those with G-type giants have solar metallicity and s-process enhancement (Smith et al. 2001a; Pereira et al. 2005).

This is the second in a series of papers on the chemical abundance analysis of the symbiotic giants. Mikołajewska et al. (2014, hereafter Paper I) discuss additional motivations for this work as well as the abundance analysis for the M star in two classical S-type symbiotic systems, RW Hya and SY Mus. In this paper, we obtain photospheric abundances for the M giant in four more symbiotic systems: AE Ara, BX Mon, KX TrA, and CL Sco. We also make a concise comparative analysis of our present and previous results.

* E-mail: cgalan@camk.edu.pl

Table 1. Journal of spectroscopic observations. Velocity parameters^a of the cool components obtained via cross-correlation technique and orbital phases calculated according to the literature ephemeris are also shown.

	Sp. Region Band($\lambda[\mu\text{m}]$)	Date	HJD(mid)	$(V_{\text{rot}}^2 \sin^2 i + \xi_t^2)^{0.5}$	V_{rad}	Orbital phase ^b
AE Ara	<i>H</i> (~1.56)	17.02.2003	2452687.8830	7.76	-6.34 ± 0.56	0.05
	<i>K</i> (~2.23)	20.04.2003	2452749.8669	9.16	-4.47 ± 0.54	0.13
	<i>K</i> (~2.23)	03.04.2004	2453098.8487	10.35	-15.30 ± 0.67	0.56
BX Mon	<i>H</i> (~1.56)	16.02.2003	2452686.7409	6.08	25.36 ± 0.48	0.30
	<i>K</i> (~2.23)	20.04.2003	2452749.5231	7.58	24.12 ± 0.40	0.35
	<i>K_r</i> (~2.36)	03.04.2006	2453828.5095	8.44	27.33 ± 0.56	0.20
KX TrA	<i>H</i> (~1.56)	17.02.2003	2452687.8230	6.05	-125.09 ± 1.92	0.73
	<i>K</i> (~2.23)	20.04.2003	2452749.7670	6.29	-126.13 ± 0.87	0.78
	<i>K</i> (~2.23)	03.04.2004	2453098.7314	5.74	-122.20 ± 1.29	0.03
CL Sco	<i>H</i> (~1.56)	17.02.2003	2452687.8341	7.02	-31.90 ± 0.68	0.07
	<i>K</i> (~2.23)	20.04.2003	2452749.7780	6.99	-32.99 ± 0.36	0.17
	<i>K</i> (~2.23)	15.08.2003	2452866.5367	8.52	-32.94 ± 0.50	0.36
	<i>K</i> (~2.23)	03.04.2004	2453098.7794	8.83	-46.51 ± 0.80	0.73

^a Units km s^{-1} .^b Orbital phase calculated from the following ephemerides: AE Ara 2453449+803.4×E (Fekel et al. 2010), BX Mon 2449796+1259×E (Fekel et al. 2000), KX TrA 2453053+1350×E (Ferrer et al. 2003), CL Sco 2452018+625×E (Fekel et al. 2007). The zero-point corresponds to the inferior conjunction of the red giant.**Table 2.** Stellar parameters, T_{eff} and $\log g$ estimated from spectral types and $T_{\text{eff}}-\log g-\text{colour}$ relation.

	AE Ara	BX Mon	KX TrA	CL Sco
Sp. Type ^[1]	M5.5	M5	M6	M5
$T_{\text{eff}}[\text{K}]^{[2]}$	3300 ± 75	3355 ± 75	3240 ± 75	3355 ± 75
$T_{\text{eff}}[\text{K}]^{[3]}$	3312	3367	3258	3367
$J - K^{[4,5]}$	1.36	1.37	1.39	1.29
$E(B - V)^{[6]}$	0.19–0.25	0.12–0.16	0.13–0.23	0.26–0.34
$(J - K)_0$	~1.25	~1.29	~1.3	~1.15
$T_{\text{eff}}[\text{K}]^{[7]}$	<3500	<3500	<3500	3500–3600
$\log g^{[7]}$	<0.39	<0.39	<0.39	~0.49
$T_{\text{eff}}[\text{K}]^a$	3300	3400	3300	3400
$\log g^a$	0.0	0.0	0.0	0.5
M_{bol}^b	-3.6	-4.1	-3.9	~-3.0

References: spectral types are from ^[1]Mürset & Schmid (1999), total Galactic extinction adopted according to ^[6]Schlaflly & Finkbeiner (2011) and Schlegel et al. (1998), infrared colours are from 2MASS ^[4](Phillips 2007) transformed to ^[5]Bessell & Brett (1988) photometric system.Callibration by: ^[2]Richichi et al. (1999), ^[3]Van Belle et al. (1999), ^[7]Kucinskis et al. (2005).^a: adopted.^b: based on known radii and/or pulsation properties.

2 OBSERVATIONS AND DATA REDUCTION

High-resolution ($R = \lambda/\Delta\lambda \sim 50000$), high-S/N ratio ($\gtrsim 100$), near-IR spectra were observed with the Phoenix cryogenic echelle spectrometer on the 8 m Gemini South telescope in 2003–2006. All the spectra cover narrow spectral intervals ($\sim 100\text{\AA}$) located in the *H* and *K* photometric bands at mean wavelengths 1.563, 2.225, and 2.361 μm (hereafter *H*, *K*, and *K_r*-band spectra, respectively). The *H*-band spectra contain molecular CO and OH lines and *K*-band spectra CN lines. In both these ranges numerous, strong atomic lines are present. These lines were used to determine abundances of carbon, nitrogen, and oxygen and elements around the iron peak:

Table 3. Quadrature sums of the projected rotational velocities and micro-turbulence $(V_{\text{rot}}^2 \sin^2 i + \xi_t^2)^{0.5}$ from *K*-band Ti I, Fe I, and Sc I lines.^a

	AE Ara	BX Mon	KX TrA	CL Sco
Apr 2003	10.06 ± 0.32	8.67 ± 0.47	8.48 ± 0.59	7.84 ± 0.60
Aug 2003	–	–	–	8.02 ± 0.54
Apr 2004	10.58 ± 0.48	–	8.94 ± 0.71	8.42 ± 0.50
all together ^b	10.30 ± 0.28	8.67 ± 0.47	8.71 ± 0.44	8.09 ± 0.29

^a Units km s^{-1} ^b Used for synthetic spectra calculations

Sc, Ti, Fe, Ni. The *K_r*-band spectra are dominated by strong CO features that enable measurement of the $^{12}\text{C}/^{13}\text{C}$ isotopic ratio. The spectra were extracted and wavelength calibrated using standard reduction techniques (Joyce 1992). The wavelength scales of all spectra were heliocentric corrected. In all cases, telluric lines were either not present in the interval observed or were removed by reference to a hot standard star. The Gaussian instrumental profile is in all cases about 6 km s^{-1} FWHM (full width at half-maximum) corresponding to instrumental profiles of 0.31, 0.44, and 0.47 \AA in the case of the *H*-, *K*-, and *K_r*-band spectra, respectively. The journal of our spectroscopic observations is given in the Table 1.

3 METHODS

Abundance analyses were performed by fitting synthetic spectra to the observed spectra using the same methods adopted in Paper I for the analyses of RW Hya and SY Mus. The technique is very similar to that used by Schmidt et al. (2006) in determining the CH Cyg abundances. Standard LTE analysis and MARCS model atmospheres by Gustafsson et al. (2008) were used for the spectral synthesis. The code WIDMO developed by Schmidt et al. (2006), was used to calculate synthetic spectra over the entire observed spectral region. To perform the χ^2 minimization a special overlay

was developed on the WIDMO code with use of the simplex algorithm (Brandt 1998). This procedure enables an improvement of the computation efficiency by a factor of ten. The atomic data were taken from the VALD database (Kupka et al. 1999) in the case of K - and K_r -band regions and from the list given by Mélendez & Barbuy (1999) for the H -band region. For the molecular data we used the lists Goorvitch (1994) for CO and Kurucz (1999) for ^{12}CN and OH. The complete list of the lines selected for our abundance analysis with excitation potentials (EP) and gf -values is shown in Tables B1 and B2 in the online Appendix B.

The input effective temperatures T_{eff} were estimated (Table 2) from the known spectral types (Mürset & Schmid 1999) adopting the calibrations by Richichi et al. (1999) and Van Belle et al. (1999). The infrared intrinsic colours derived from the 2MASS (Phillips 2007) magnitudes and colour excesses (Schlafly & Finkbeiner 2011, Schlegel et al. 1998) combined with the Kucinkas et al. (2005) $T_{\text{eff}}\text{--}\log g\text{--}\text{colour}$ relation for late-type giants resulted in surface gravities and effective temperatures that are in good agreement with those from the spectral types. The adopted model atmospheres had effective temperatures $T_{\text{eff}} = 3300\text{ K}$ for AE Ara and KX TrA and 3400 K for CL Sco and BX Mon. $\log g = 0$ with the exception of CL Sco where $\log g$ was set to 0.5. It is difficult to estimate uncertainty in the adopted $\log g$, however, it should not be larger than ~ 0.5 which is the resolution of the MARCS model atmosphere grid used in our calculation. In the case of BX Mon, an additional constraint on the $\log g$ can be obtained using the red giant mass, $M_g = 3.7 \pm 1.9 M_{\odot}$, and radius, $R_g = 160 \pm 50 R_{\odot}$ derived by Dumm et al. (1998). The resulting $\log g = 0.6^{+0.5}_{-0.6}$. Using the significantly improved orbital solution (Brandt 2009), the red giant mass is $M_g \sim 1.5 M_{\odot}$, and the resulting $\log g \sim 0.2$, in good agreement with the value(s) adopted in our study. The macroturbulence velocity ζ_1 was set at 3 km/s , a value typical for the cool red giants (e.g. Fekel et al. 2003).

To obtain radial and rotational velocities, we used a cross-correlation technique similar to that adopted by Carlberg et al. (2011) but using synthetic spectra as the templates. The method is described in detail in Paper I and the obtained values are presented in Table 1. The rotational velocities were additionally estimated (Table 3) via direct measurement of the FWHM of the six relatively strong unblended atomic lines (Ti I, Fe I, Sc I) present in the K -band region. The same lines were used by Fekel et al. (2003) to measure the rotational velocities in roughly a dozen symbiotic systems. We used the radial velocities obtained by cross-correlation (Table 1) and rotational velocities obtained from atomic lines in K -band spectra (Table 3) as fixed parameters in our solutions.

A detailed description of the methods used to estimate the input parameters and to derive the abundance solution was presented in Paper I. A brief outline follows. Values of the abundance parameters (C, N, O, Sc, Ti, Fe, Ni) were initially set to the solar composition (Asplund et al. 2009). Abundances of the oxygen, carbon, nitrogen, and iron peak elements were adjusted by fitting by eye, alternately from the OH, CO, CN, and atomic lines, over several iterations. Next, the initial grid of the $n+1, n$ dimensional sets of free parameters, the so-called simplex needed for the simplex algorithm, was prepared. Nine different simplexes were used with different microturbulent velocity ξ_1 values sampled in the range $1.2\text{--}2.6\text{ km/s}$ to obtain best fits to H - and K -band spectra. For three objects (AE Ara, KX TrA, and CL Sco) for which we do not have the K_r -band spectrum the $^{12}\text{C}/^{13}\text{C}$ isotopic ratio was set to 8, a value close to the average for our objects with known isotopic ratios. For BX Mon after we found the sets of parameters that give the best fit to the H - and K -band spectra, we applied these abundances to the K_r -band

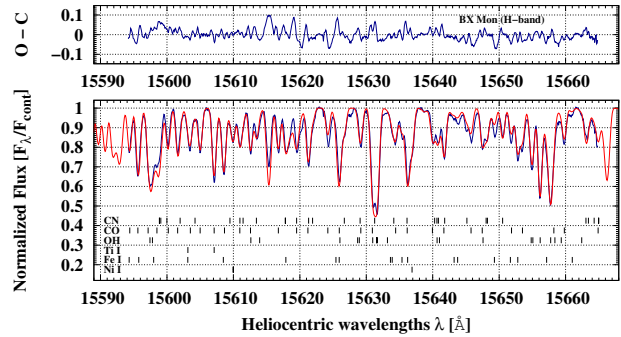


Figure 1. The spectrum of BX Mon observed in 2003 February (blue line) in the H band and a synthetic spectrum (red line) calculated using the final abundances and $^{12}\text{C}/^{13}\text{C}$ isotopic ratio (Table 4).

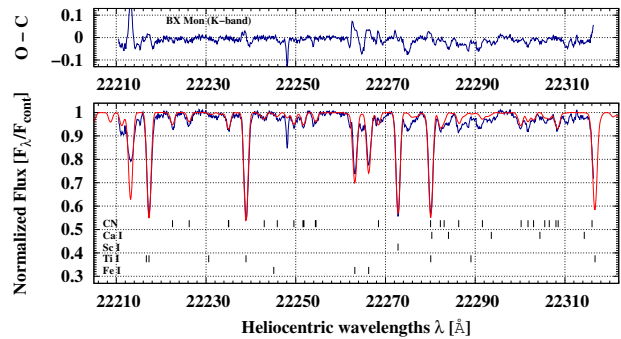


Figure 2. The spectrum of BX Mon observed in 2003 April (blue line) in the K band and a synthetic spectrum (red line) calculated using the final abundances and $^{12}\text{C}/^{13}\text{C}$ isotopic ratio (Table 4).

spectrum as a fixed parameter and searched for $^{12}\text{C}/^{13}\text{C}$ isotopic ratio. After obtaining the optimal fit, we made a reconciliation of ^{12}C and $^{12}\text{C}/^{13}\text{C}$ in three iterations.

4 RESULTS

Table 4 summarizes the final abundances and formal uncertainties derived from CNO molecules and atomic lines (Sc I, Ti I, Fe I, Ni I) on the scale of $\log \epsilon(X) = \log N(X)N(H)^{-1} + 12.0$, the isotopic ra-

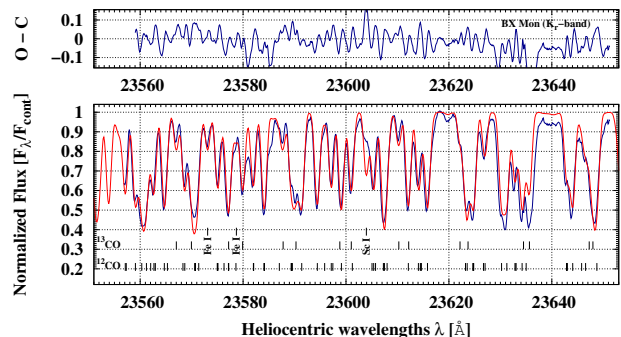


Figure 3. The spectrum of BX Mon observed in 2006 April (blue line) in the K_r band and a synthetic spectrum (red line) calculated using the final abundances and $^{12}\text{C}/^{13}\text{C}$ isotopic ratio (Table 4).

Table 4. Calculated abundances and relative abundances,^a velocity parameters,^b and uncertainties^c for AE Ara, BX Mon, KX TrA, and CL Sco.

<i>X</i>	AE Ara		BX Mon		KX TrA		CL Sco	
	log $\epsilon(X)$	[<i>X</i>]	log $\epsilon(X)$	[<i>X</i>]	log $\epsilon(X)$	[<i>X</i>]	log $\epsilon(X)$	[<i>X</i>]
¹² C	8.10±0.02	-0.33±0.07	7.79±0.02	-0.64±0.07	8.03±0.02	-0.40±0.07	8.02±0.04	-0.41±0.09
N	8.15±0.06	+0.32±0.11	7.89±0.04	+0.06±0.09	8.04±0.06	+0.21±0.11	8.14±0.13	+0.31±0.18
O	8.64±0.04	-0.05±0.08	8.37±0.03	-0.32±0.07	8.66±0.05	-0.03±0.10	8.61±0.06	-0.08±0.11
Sc	4.53±0.24	+1.38±0.28	3.82±0.26	+0.67±0.30	4.02±0.18	+0.87±0.22	3.47±0.25	+0.32±0.29
Ti	5.40±0.12	+0.45±0.17	4.96±0.15	+0.01±0.20	5.08±0.17	+0.13±0.22	4.93±0.22	-0.02±0.27
Fe	7.41±0.06	-0.09±0.10	7.16±0.06	-0.34±0.10	7.17±0.03	-0.33±0.07	7.21±0.09	-0.29±0.13
Ni	6.28±0.18	+0.06±0.22	6.18±0.13	-0.04±0.17	6.21±0.09	-0.01±0.13	6.23±0.10	+0.01±0.14
¹² C/ ¹³ C	—	—	8±1	—	—	—	—	—
ξ_t	1.7±0.2		1.8±0.2		1.9±0.2		1.9±0.3	
$V_{\text{rot}} \sin i$	10.2±0.3		8.5±0.5		8.5±0.5		7.9±0.3	

^a Relative to the Sun [*X*] abundances estimated in relation to the solar composition of Asplund et al. (2009)^b Units km s⁻¹^c 3 σ **Table 5.** Sensitivity of abundances to uncertainties in the stellar parameters

ΔX	$\Delta T_{\text{eff}} = +100 \text{ K}$	$\Delta \log g = +0.5$	$\Delta \xi_t = +0.5$	$\Delta [Fe/H] = +0.25$
C	+0.02	+0.22	-0.08	+0.05
N	+0.04	+0.02	-0.11	+0.07
O	+0.13	+0.08	-0.12	+0.12
Sc	+0.12	+0.20	-0.69	-0.01
Ti	+0.07	+0.16	-0.52	+0.02
Fe	-0.05	+0.16	-0.17	-0.02
Ni	-0.07	+0.20	-0.22	-0.02

tio ¹²C/¹³C (only in the case of BX Mon), microturbulences, ξ_t , and projected rotational velocities, $V_{\text{rot}} \sin i$. The abundance of scandium is based on only one strong Sc I line at $\lambda \sim 22272.8 \text{ \AA}$ and may be less reliable than other abundances presumably due to the broadening of the infrared scandium lines by hyperfine structure that has not been included in the analysis (see Paper I). The synthetic fits to the observed spectra of BX Mon are shown in Figures 1-3, where the molecular (OH, CO, CN) and atomic (Sc I, Ti I, Fe I, Ni I) lines used in the solution of the chemical composition are identified by ticks. Synthetic fits to the observed spectra of AE Ara, KX TrA, and CL Sco in *H*- and *K*-band regions are shown in Figures A1-A6 in the online Appendix A.

We also made fits with MARCS atmosphere models varying the effective temperatures by $\pm 100 \text{ K}$, $\log g$ by ± 0.5 , and the microturbulence (ξ_t) by ± 0.5 to estimate the sensitivity of abundances to uncertainties in stellar parameters. In the case of AE Ara and CL Sco additional fits were also made using models with [Fe/H] different by $+0.25$. The changes in the abundance for each element as a function of each model parameter are listed in Table 5. Uncertainties in the stellar parameters have a stronger impact on the uncertainty of the derived chemical composition than the uncertainties from fitting the synthetic spectrum.

In our solution, the microturbulence velocity was treated as free parameter. In all cases, we obtained microturbulence values close to 2. Abundances of some elements strongly depend on the microturbulence value. Smith et al. (2002) showed that for red giants microturbulence is correlated with bolometric magnitudes. We repeated the analysis for BX Mon, AE Ara, KX TrA, and CL Sco adopting the microturbulence values, 2.5, 2.5, 2.5, and 2.3, respectively, corresponding to their bolometric magnitudes (Table 2). The

resulting abundances and their sensitivity on the changes in the stellar parameters are presented in Tables 6 and 7, respectively. These new abundances are shifted towards somewhat lower (by ~ 0.2 dex) metallicities. In particular, for all objects we obtained sub-solar metallicities, [Fe/H] ~ -0.3 to -0.55 . For BX Mon, we also calculated abundances for $\log g = +0.5$.

5 DISCUSSION

Here, we present the first ever analysis of the photospheric chemical abundances (CNO and elements around the iron peak: Sc, Ti, Fe, and Ni) for four classical S-type symbiotic systems: AE Ara, BX Mon, KX TrA, and CL Sco. Our analysis reveals an approximately solar metallicity for AE Ara and slightly sub-solar metallicities ([Fe/H] ~ -0.3) for BX Mon, KX TrA, and CL Sco. The CNO abundances are similar to typical values derived for single Galactic M giants. In particular, they all show carbon depletion and nitrogen enhancement (Smith & Lambert 1990). The ratio of ¹²C/¹³C ~ 8 obtained for BX Mon is very similar to the values of ¹²C/¹³C ~ 6 and 10 derived for RW Hya and SY Mus (Paper I). The CNO values and isotopic ratios indicate that the red giants in these systems have experienced the first dredge-up.

Relative abundances of C/N/O for these systems were previously derived based on nebular emission lines in ultraviolet spectra by Nussbaumer et al. (1988) and Pereira (1995). Pereira (1995) also estimated Fe/O from optical emission lines. A comparison of these estimates with our present results and those from Paper I is shown in Table 8. The abundances from emission lines should be most reliable when based on spectra taken during superior conjunction of the cool giant ($\phi \sim 0.5$) when the hot component and the nebula are visible in front of the giant. This was the case for KX TrA, AE Ara, and BX Mon and perhaps SY Mus. The C/O ratios obtained using emission line technique are in fairly good agreement with our photospheric values especially for KX TrA and AE Ara. For the other objects the differences are bigger. In the case of BX Mon, the difference is likely due to poor quality of the *IUE* spectrum used by Nussbaumer et al. (1988). The *IUE* spectra of CL Sco and RW Hya were taken relatively close to the inferior conjunction of the red giant when the emission lines are affected by eclipse and Rayleigh scattering effects. Nussbaumer et al. (1988) also noted that their method may systematically underestimate the

Table 6. Calculated abundances and relative abundances,^a velocity parameters,^b and uncertainties^c for AE Ara, BX Mon, KX TrA, and CL Sco. The case for fixed microturbulences.

X	AE Ara		BX Mon		BX Mon ^d		KX TrA		CL Sco	
	log $\epsilon(X)$	[X]	log $\epsilon(X)$	[X]	log $\epsilon(X)$	[X]	log $\epsilon(X)$	[X]	log $\epsilon(X)$	[X]
¹² C	7.93±0.03	-0.50±0.08	7.66±0.03	-0.77±0.08	7.87±0.03	-0.56±0.08	7.89±0.03	-0.54±0.07	7.92±0.04	-0.51±0.09
N	7.89±0.09	+0.06±0.14	7.65±0.06	-0.18±0.11	7.67±0.05	-0.16±0.10	7.82±0.09	-0.01±0.14	7.96±0.10	+0.13±0.15
O	8.35±0.03	-0.34±0.07	8.14±0.01	-0.55±0.06	8.23±0.02	-0.46±0.06	8.39±0.05	-0.30±0.10	8.39±0.03	-0.30±0.08
Sc	3.45±0.22	+0.30±0.25	3.15±0.22	+0.00±0.26	3.29±0.18	+0.14±0.22	3.33±0.12	+0.18±0.16	3.16±0.23	+0.01±0.27
Ti	4.55±0.08	-0.40±0.13	4.33±0.06	-0.62±0.11	4.48±0.07	-0.47±0.12	4.46±0.12	-0.49±0.17	4.53±0.12	-0.42±0.17
Fe	7.16±0.06	-0.34±0.10	6.95±0.04	-0.55±0.08	7.10±0.04	-0.40±0.08	6.96±0.06	-0.54±0.10	7.07±0.08	-0.43±0.12
Ni	5.95±0.09	-0.27±0.13	5.93±0.10	-0.29±0.14	6.09±0.08	-0.13±0.12	5.96±0.08	-0.26±0.12	6.11±0.10	-0.11±0.14
¹² C/ ¹³ C	—	—	12±2	—	11±1	—	—	—	—	—
ξ_t	2.5		2.5		2.5		2.5		2.3	
$V_{\text{rot}} \sin i$	10.0±0.3		8.3±0.5		8.3±0.5		8.3±0.5		7.8±0.3	

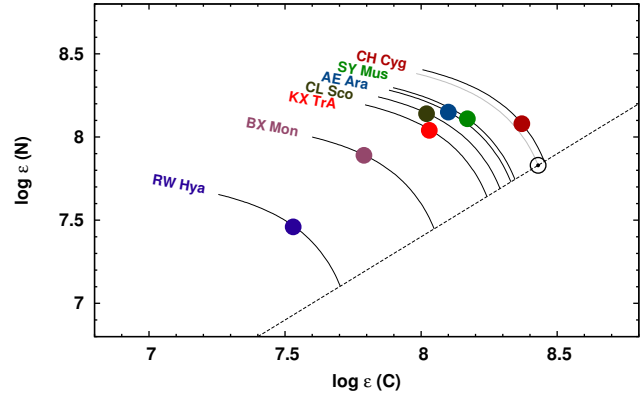
^a Relative to the Sun [X] abundances estimated in relation to the solar composition of Asplund et al. (2009)^b Units km s⁻¹^c 3 σ ^d log $g = 0.5$ **Table 7.** Sensitivity of abundances to uncertainties in the stellar parameters. The case for fixed microturbulences.

ΔX	$\Delta T_{\text{eff}} = +100 \text{ K}$	$\Delta \log g = +0.5$	$\Delta \xi_t = +0.5$
C	+0.02	+0.22	-0.04
N	+0.02	+0.03	-0.12
O	+0.10	+0.10	-0.09
Sc	+0.10	+0.16	-0.38
Ti	+0.06	+0.17	-0.39
Fe	-0.05	+0.17	-0.19
Ni	-0.05	+0.18	-0.17

C and O abundances relative to the N abundance and this effect in the worst cases may reach 30 per cent.

The elemental abundances of the symbiotic giants summarized in Table 9 can be used to address evolutionary status and to associate symbiotic systems with stellar populations of the Milky Way. In particular the C and N abundances are very good monitors of dredge-up on the RGB provided that only the CN cycle has operated significantly in the dredged material. In such a case, the total number of C+N nuclei should be conserved since ¹²C will be converted to ¹⁴N. Cunha & Smith (2006) showed that the Galactic bulge giants behave in good agreement with the simple CN mixing picture. Paper I demonstrated the same behaviour of the red giants in RW Hya, SY Mus, and CH Cyg. Fig. 4 show the ¹⁴N versus ¹²C abundances for the symbiotic sample so far analysed. All symbiotic giants fall into the ¹⁴N-enhanced zone providing a very strong indication that they have experienced the first dredge-up. This is also confirmed by the low ¹²C/¹³C isotopic ratios for those stars with measured values.

Thus, we can assume, as did Cunha & Smith (2006) for their sample of the bulge giants, that the O and Fe and other elemental abundances roughly represent the original values with which the symbiotic stars were born. These abundances can then be used to identify the parent Galactic population. The ratio of α -elements (e.g. O and Ti in our study) to Fe is of particular importance because the α -element originate mostly from massive stars and SNe II, and they are produced over relatively short time-scales whereas Fe is most effectively produced in SNe Ia over much longer

**Figure 4.** Nitrogen versus carbon for the symbiotic giants. The dashed line represents scaled solar abundances, [¹²C/Fe]=0 and [¹⁴N/Fe]=0, whereas the solid curves delineate constant ¹²C+¹⁴N.

time-scales. Thus, differences in contamination by SNe II and SNe Ia lead to significantly different trends for particular populations, and their clear separation in the [O/Fe] versus [Fe/H] plane (e.g. Cunha & Smith 2006, Bensby & Feltzing 2006).

Figure 5 shows [O/Fe] versus [Fe/H] of the symbiotic giants along with the values for various stellar populations taken from a number of studies (Edvardsson et al. 1993, Prochaska et al. 2000, Mélenlez et al. 2001, Smith et al. 2001b, Mélenlez 2002, Fulbright & Johnson 2003, Reddy et al. 2003, Rich & Origlia 2005, Bensby et al. 2005, Cunha & Smith 2006, Alves-Brito et al. 2010, Ryde et al. 2010, Rich et al. 2012, Smith et al. 2013) and scaled to the solar composition of Asplund et al. (2009). We have distinguished four populations: thin and thick discs, halo, and bulge. Part of the bulge population containing objects from Baade's Windows and from two other nearby inner bulge fields F175 and F265 (Rich & Origlia 2005; Rich et al. 2012) is highlighted with red. These objects are more chemically homogeneous than the rest of the bulge sample as indicated by their grouping in a small area of the diagram. The rest of the sample contains objects spread in the bulge (Cunha & Smith 2006; Alves-Brito et al. 2010; Ryde et al. 2010) and is more representative for the whole bulge population.

Table 8. Comparison of our photospheric abundances with those derived using emission line technique.

Object	C/N	O/N	C/O	Fe/O	Phase ^a	Ref.
KX TrA	1.59	4.42	0.36	0.046	0.52	[3]
	2.28	6.91	0.33	–	0.27	[3]
	0.98	4.17	0.23	0.032		[1]
AE Ara	1.2	3.7	0.32	–	0.43	[4]
	0.89	3.09	0.29	0.059		[1]
BX Mon	0.29	2.0	0.15	–	0.49	[4]
	0.79	3.02	0.26	0.062		[1]
CL Sco	0.77	5.7	0.14	–	0.87	[4]
	0.76	2.95	0.26	0.040		[1]
SY Mus	0.97	1.9	0.51	–	0.36	[4]
	1.15	3.55	0.32	0.058		[2]
RW Hya	0.42	1.7	0.25	–	0.15	[4]
	1.17	5.13	0.23	0.037		[2]

References: ^[1] this work, ^[2] Paper I, ^[3] Pereira (1995), ^[4] Nussbaumer et al. (1988).

^a Orbital phase the same as in Table 1, and table 2 in Paper I.

Table 9. Absolute and relative abundances adopted for the comparison with the Galactic stellar populations. Two cases for the microturbulence being free and fixed parameter are shown at the top and at the middle, respectively. Abundances of RW Hya and SY Mus from Paper I and CH Cyg and V2116 Oph from the literature are shown for comparison at the bottom.

Object	$A(^{12}\text{C})$	$A(^{14}\text{N})$	[O/Fe]	[Fe/H]	ξ_t
AE Ara	8.10	8.15	+0.04	-0.09	1.7
	7.93	7.89	+0.00	-0.34	2.5
BX Mon	7.79	7.89	+0.02	-0.34	1.8
	7.66	7.65	+0.00	-0.55	2.5
KX TrA	7.87	7.67	-0.06	-0.40	2.5 ^a
	8.03	8.04	+0.30	-0.33	1.9
CL Sco	7.89	7.82	+0.24	-0.54	2.5
	8.02	8.14	+0.21	-0.29	1.9
RW Hya ^[1]	7.92	7.96	+0.13	-0.43	2.3
	7.53	7.46	+0.24	-0.76	1.8
SY Mus ^[1]	8.17	8.11	+0.05	-0.08	2.0
CH Cyg ^[2]	8.37	8.08	+0.07	+0.00	2.2
V2116 Oph ^[3]	8.03	8.97	-0.22	-0.05	2.4

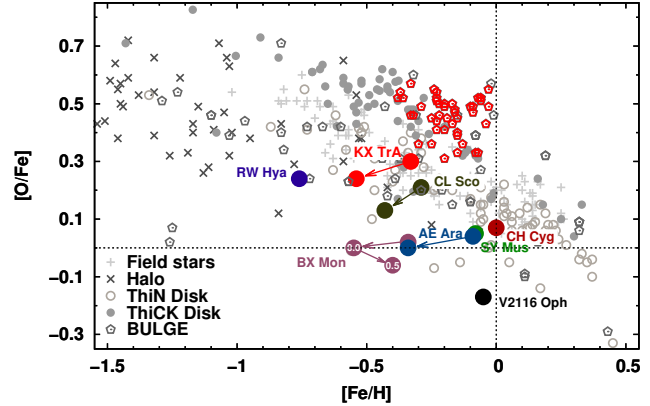
References: ^[1] Paper I, ^[2] Schmidt et al. (2006), ^[3] Hinkle et al. (2006).

^a $\log g = 0.5$

The thin and thick disc samples contain only those objects with membership confirmed by their kinematic characteristics. Finally, the 'field star' group represents the objects for which there is no kinematic information about their population membership. It may contain stars from all Galactic populations but it seems to be dominated by the thin disc members.

The position in the [O/Fe]–[Fe/H] plane of the objects studied here can be related to membership in Galactic populations. Most appear to belong to the Galactic disc or bulge while the position of RW Hya supports its membership in the extended thick-disc/halo population. Additional independent methods, e.g. simultaneous kinematic studies on the Toomre diagram (Feltzing et al. 2003; Gałan et al. 2014), are necessary to sort out this question. Such studies will be performed in the near future on a more statistically significant sample.

In the process of fitting the synthetic spectra we measured radial and rotational velocities for the programme stars (Tables 1 and

**Figure 5.** Oxygen relative to iron for various stellar populations with positions of our targets denoted with large coloured circles. The results of additional calculations with fixed microturbulence values are designated by arrows (for BX Mon two values of $\log g = 0$ and $+0.5$ were used).

3). Radial velocities obtained for three objects, AE Ara, BX Mon, and CL Sco, using cross-correlation techniques are consistent with recent spectroscopic orbits published for these stars. Radial velocities obtained for AE Ara are in agreement with results obtained with the same spectra by Fekel et al. (2010) with discrepancies no larger than 2 km s^{-1} . Residuals calculated by Fekel et al. (2010) from the synthetic orbit are within the range $\sim 1.5\text{--}2 \text{ km s}^{-1}$. Similarly the radial velocities obtained for CL Sco agree with values obtained by the Fekel et al. (2007) with the same spectra with differences in the range $\sim 0.2\text{--}2.3 \text{ km s}^{-1}$. Residuals from the synthetic orbit calculated by Fekel et al. (2007) have values between $\sim 1\text{--}3 \text{ km s}^{-1}$. Radial velocities obtained for BX Mon are in accord with synthetic radial velocities predicted from the orbit of Fekel et al. (2000) with an accuracy generally better than $\sim 2 \text{ km s}^{-1}$. In the case of KX TrA, however, we could not achieve agreement with published orbits. The range of the velocities measured by us, -122 to -126 km s^{-1} , is covered by the γ velocity of -123.7 km s^{-1} and K of 6.8 km s^{-1} found by Ferrer et al. (2003) but computed versus observed velocities are not consistent with an orbital period of 1350 d. The orbit of Harries & Howarth (2000) from spectropolarimetric observation is similar to that of Ferrer et al. (2003). The Marchiano et al. (2008) orbit is similar but the 1916 d period is significantly longer. Further study and possibly recalculation with another period is needed.

Giants in symbiotic stars are characterized with large rotational velocities and in all the systems studied by us so far $V_{\text{rot}} \sin i$ makes the largest contribution to the physical line broadening. The rotational velocities obtained with the cross-correlation method generally have smaller values than obtained with FWHM method (Tables 1 and 3). The rotational velocities obtained from strongly blended spectra with strong molecular lines (like H -band spectra) appear to be significantly underestimated, and the use of rotational velocities as a free parameters does not lead to significant differences in obtained values of the rotational velocities and abundances (Paper I). Therefore, our analysis used velocities obtained with FWHM method that gives more self-consistent results in accord with those obtained from the same spectra with cross-correlation method.

6 CONCLUSIONS

We have performed a detailed analysis of the photospheric abundances of CNO and elements around the iron peak (Sc, Ti, Fe, and Ni) for the red giant components of the S-type symbiotic binaries: AE Ara, BX Mon, KX TrA, and CL Sco. Our analysis revealed a near-solar metallicity for AE Ara, and slightly sub-solar metallicities ($[\text{Fe}/\text{H}] \sim -0.3$) for BX Mon, KX TrA, and CL Sco. However, the metallicities are lower by ~ 0.2 dex when the microturbulence values were estimated from bolometric magnitudes instead of keeping the microturbulence as a free parameter. The enrichment in ^{14}N isotope obtained for all these objects indicates that the giants have experienced the first dredge-up which is also confirmed by the very low $^{12}\text{C}/^{13}\text{C}$ isotopic ratio ~ 8 obtained for BX Mon.

ACKNOWLEDGEMENTS

This study has been supported in part by the Polish NCN grant no. DEC-2011/01/B/ST9/06145. CG has been also financed by the NCN postdoc programme FUGA via grant DEC-2013/08/S/ST9/00581. The observations were obtained at the Gemini Observatory, which is operated by the Association of Universities for Research in Astronomy, Inc., under a cooperative agreement with the NSF on behalf of the Gemini partnership: the National Science Foundation (United States), the National Research Council (Canada), CONICYT (Chile), the Australian Research Council (Australia), Ministério da Ciência, Tecnologia e Inovação (Brazil) and Ministerio de Ciencia, Tecnología e Innovación Productiva (Argentina). CG is thankful to Mirosław Schmidt for his valuable and useful comments.

REFERENCES

- Alves-Brito, A., Meléndez, J., Asplund, M., et al., 2010, *A&A*, 513, 35
- Angeloni, R., Di Mille, F., Bland-Hawthorn, J., et al., 2011, *ApJ*, 743, 8
- Asplund, M., Grevesse, N., Sauval, A., & Scott, P., 2009, *ARAA* 47, 481
- Bensby, T., Feltzing, S., Lundström, I., Ilyin, I., 2005, *A&A*, 433, 185
- Bensby, T., & Feltzing, S., 2006, *MNRAS*, 367, 1181
- Bessell, M. S., & Brett, J. M., 1988, *PASP*, 100, 1134
- Brandi, E., García, L. G., Quiroga, C., et al., 2009, *BAAA*, 52, 49
- Brandt, S., Data Analysis, Statistical and Computational Methods, 1998, Polish edition. Polish Scientific Publishers PWN, Warsaw
- Carlberg, J. K., Majewski, S. R., Patterson, R. J., et al., 2011, *ApJ*, 732, 39
- Cunha, K., & Smith, V. V., 2006, *ApJ*, 651, 491
- Dilday, B., Howell, D. A., Cenko, S. B., et al., 2012, *Science*, 337, 942
- Dumm, T., Mürset, U., Nussbaumer, H., et al., 1998, *A&A*, 336, 637
- Edvardsson, B., Andersen, J., Gustafsson, B., et al., 1993, *A&A*, 275, 101
- Fekel, F. C., Joyce, R. R., Hinkle, K. H., Skrutskie, M. F., 2000, *AJ*, 119, 1375
- Fekel, F. C., Hinkle, K. H., Joyce, R. R., 2003, Corradi R. L. M., Mikolajewska R., Mahoney T. J., eds, ASP Conf. Ser. Vol. 303, Symbiotic Stars Probing Stellar Evolution. Astron. Soc. Pac., San Francisco, p. 113
- Fekel, F. C., Hinkle, K. H., Joyce, R. R., et al., 2007, *AJ*, 133, 17
- Fekel, F. C., Hinkle, K. H., Joyce, R. R., Wood, P. R., 2010, *AJ*, 139, 1315
- Feltzing, S., Bensby, T., Lundström, I., 2003, *A&A*, 397, 1
- Ferrer, O., Quiroga, C., Brandi, E., García, L. G., 2003, in Corradi R. L. M., Mikolajewska R., Mahoney T. J., eds, ASP Conf. Ser. Vol. 303, Symbiotic Stars Probing Stellar Evolution. Q12 Astron. Soc. Pac., San Francisco, p. 117
- Fulbright, J. P., & Johnson, J. A., 2003, *ApJ*, 595, 1154
- Gałań, C., Mikolajewska, J., Hinkle, K. H., et al., 2014, in Morisset C., Delgado-Inglada G., Torres-Peimbert S., eds, Proc. Asymmetrical Planetary Nebulae VI Conf., Chemical Abundance Analysis of Symbiotic Giants. RW Hya, SY Mus, BX Mon, and AE Ara. Available at: <http://www.astroscu.unam.mx/apn6/PROCEEDINGS/A22-Galan.pdf>
- Goorvitch, D., 1994, *ApJS*, 95, 535
- Gustafsson, B., Edvardsson, B., Eriksson, K., et al., 2008, *A&A*, 486, 951
- Harries, T. J., & Howarth, I. D., 2000, *A&A*, 361, 139
- Hinkle, K. H., Fekel, F. C., Joyce, R. R., et al., 2006, *ApJ*, 641, 479
- Joyce, R. 1992, in Howell S., ed., ASP Conf. Ser. Vol. 23, Astronomical CCD Observing and Reduction Techniques. Astron. Soc. Pac., San Francisco, p. 258
- Kenyon, S. J., & Mikolajewska, J., 1995, *AJ*, 110, 391
- Kucinkas, A., Hauschildt, P. H., Ludwig, H.-G., et al., 2005, *A&A*, 442, 281
- Kupka, F., Piskunov, N., Ryabchikova, T., et al., 1999, *A&AS*, 138, 119
- Kurucz, R. L., 1999, <http://kurucz.harvard.edu>
- Marchiano, P., Brandi, E., Quiroga, C., et al., 2008, *BAAA*, 51, 117
- Meléndez, J., & Barbuy, B., 1999, *ApJS*, 124, 527
- Meléndez, J., Barbuy, B., Spite, F., 2001, *ApJ*, 556, 858
- Meléndez, J., & Barbuy, B., 2002, *ApJ*, 575, 474
- Mikolajewska, J., 2012, *Baltic Astronomy*, 21, 5
- Mikolajewska, J., Gałań, C., Hinkle, K. H., et al., 2014, *MNRAS*, 440, 3016 (Paper I)
- Mürset, U., & Schmid, H. M., 1999, *A&AS*, 137, 473
- Nussbaumer, H., Schild, H. M., Schmid, H. M., Vogel, M., 1988, *A&A*, 198, 179
- Pereira, C. B., 1995, *A&A*, 111, 471
- Pereira, C. B., Smith, V. V., Cunha, K., 1998, *AJ*, 116, 1977
- Pereira, C. B., Smith, V. V., Cunha, K., 2005, *A&A*, 429, 993
- Pereira, C. B., & Roig, F., 2009, *AJ*, 137, 118
- Phillips, J. P., 2007, *MNRAS*, 376, 1120
- Podsiadlowski Ph., & Mohamed S., 2007, *Baltic Astronomy*, 16, 26
- Prochaska, J. X., Naumov, S. O., Carney, B. W., 2000, *AJ*, 120, 2513
- Reddy, B. E., Tomkin, J., Lambert, D. L., Allende Prieto, C., 2003, *MNRAS*, 340, 304
- Rich, R. M., & Origlia, L., 2005, *ApJ*, 634, 1293
- Rich, R. M., Origlia, L., Valenti, E., 2012, *ApJ*, 746, 59
- Richichi, A., Fabbri, L., Ragland, S., Scholz, M., 1999, *A&A*, 344, 511
- Ryde, N., Gustafsson, B., Edvardsson, B., et al., 2010, *A&A*, 509, 20
- Schlaflly, E. F., & Finkbeiner, D. P., 2011 *ApJ*, 737, 103
- Schlegel, D. J., Finkbeiner, D. P., Davis, M., 1998 *ApJ*, 500, 525
- Solf, J., & Ulrich, H., 1985, *A&A*, 148, 274
- Schmidt, M. R., Zacs, L., Mikolajewska, J., & Hinkle, K., 2006,

- A&A, 446, 603
 Smith, V. V., & Lambert, D., 1988, ApJ, 333, 219
 Smith, V. V., & Lambert, D., 1990, ApJS, 72, 387
 Smith, V. V., Cunha, K., Jorissen, A., Boffin, H. M. J., 1996, A&A, 315, 179
 Smith, V. V., Cunha, K., Jorissen, A., Boffin, H. M. J., 1997, A&A, 324, 97
 Smith, V. V., Pereira, C. B., Cunha, K., 2001, ApJ, 556, 55
 Smith, V. V.; Cunha, K., King, J. R., 2001, AJ, 122, 370
 Smith, V. V.; Hinkle, K. H., Cunha, K., et al., 2002, AJ, 124, 3241
 Smith, V. V., Cunha, K., Shetrone, M. D., et al., 2013, ApJ, 765, 16
 Tomov T., 2003, in Corradi R. L. M., Mikolajewska R., Mahoney T. J., eds, ASP Conf. Ser. Vol. 303, Symbiotic Stars Probing Stellar Evolution. Astron. Soc. Pac., San Francisco, p. 376
 Van Belle, G. T., Lane, B. F., Thompson, R. R., et al. 1999, AJ, 117, 521
 Wallerstein, G., Harrison, T., Munari, U., Vanture, A., 2008, PASP, 120, 492

APPENDIX A: OBSERVED AND SYNTHETIC SPECTRA OF AE ARA, KX TRA, AND CL SCO

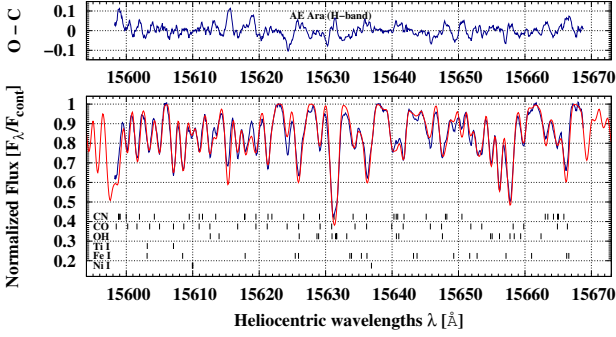


Figure A1. The spectrum of AE Ara observed in 2003 February (blue line) in the *H* band and a synthetic spectrum (red line) calculated using the final abundances (Table 4).

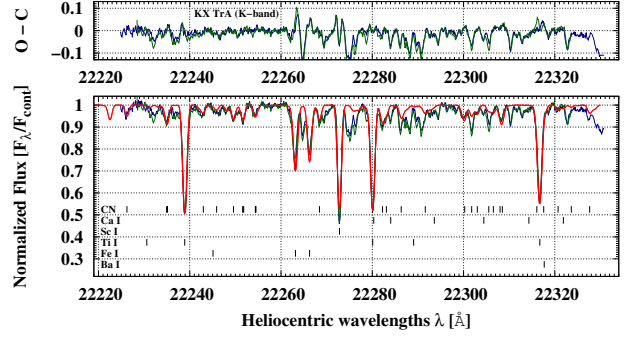


Figure A4. Spectra of KX TrA observed in 2003 April (blue line) and April 2004 (green line) in the *K* band and a synthetic spectrum (red line) calculated using the final abundances (Table 4).

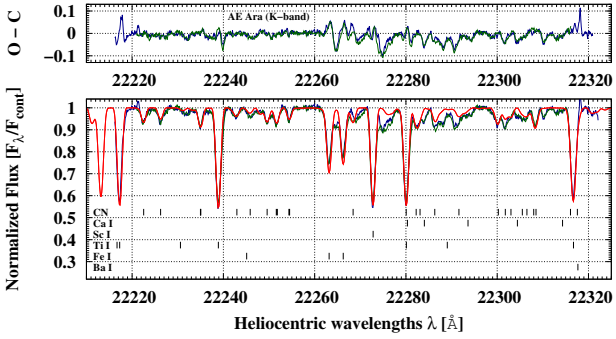


Figure A2. Spectra of AE Ara observed in 2003 April (blue line) and April 2004 (green line) in the *K* band and a synthetic spectrum (red line) calculated using the final abundances (Table 4).

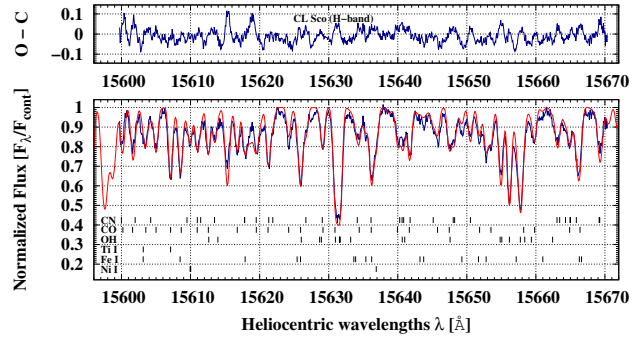


Figure A5. The spectrum of CL Sco observed in 2003 February (blue line) in the *H* band and a synthetic spectrum (red line) calculated using the final abundances (Table 4).

APPENDIX B: LIST OF ATOMIC AND MOLECULAR LINES

This paper has been typeset from a \LaTeX file prepared by the author.

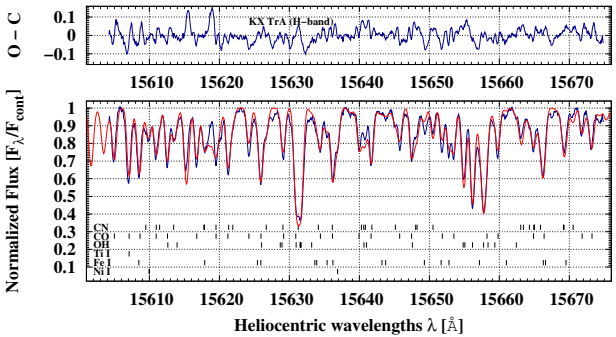


Figure A3. The spectrum of KX TrA observed in 2003 February (blue line) in the *H* band and a synthetic spectrum (red line) calculated using the final abundances (Table 4).

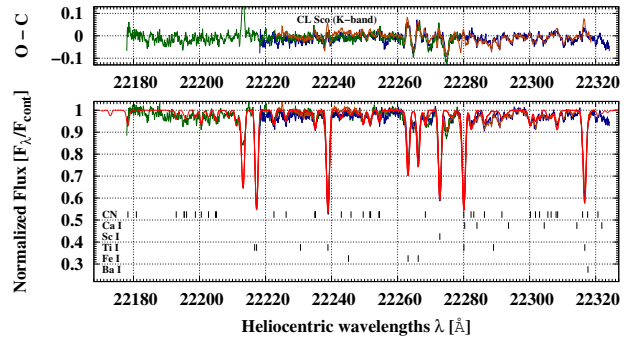


Figure A6. Spectra of CL Sco observed in 2003 April (blue line), 2003 August (green line), and April 2004 (dark-orange line) in the *K* band and a synthetic spectrum (red line) calculated using the final abundances (Table 4).

Table B1. List of atomic lines selected for calculations together with gf -values and excitation potentials.

Wavelength (air) (Å)	EP (eV)	$\log gf$	Ref.
Sc I			
^a 22202.640	1.428	-3.436	Kupka et al. (1999)
^a 22207.128	1.428	-1.836	Kupka et al. (1999)
22266.729	1.428	-1.327	Kupka et al. (1999)
^a 23603.945	1.428	-2.180	Kupka et al. (1999)
Ti I			
15598.890	4.690	-0.030	Mélendez & Barbuy (1999)
15602.840	2.270	-1.810	Mélendez & Barbuy (1999)
22210.636	4.213	-1.444	Kupka et al. (1999)
22211.228	1.734	-1.770	Kupka et al. (1999)
22224.530	4.933	-0.263	Kupka et al. (1999)
22232.838	1.739	-1.658	Kupka et al. (1999)
22274.012	1.749	-1.756	Kupka et al. (1999)
22282.973	4.690	-0.586	Kupka et al. (1999)
22310.617	1.734	-2.124	Kupka et al. (1999)
Fe I			
15590.050	6.240	-0.550	Mélendez & Barbuy (1999)
15591.490	6.240	0.360	Mélendez & Barbuy (1999)
15593.740	5.030	-1.980	Mélendez & Barbuy (1999)
15598.870	6.240	-0.920	Mélendez & Barbuy (1999)
15604.220	6.240	0.280	Mélendez & Barbuy (1999)
15613.630	6.350	-0.290	Mélendez & Barbuy (1999)
15621.160	6.200	-0.990	Mélendez & Barbuy (1999)
15621.650	5.540	+0.170	Mélendez & Barbuy (1999)
15629.370	5.950	-1.670	Mélendez & Barbuy (1999)
15629.630	4.560	-3.130	Mélendez & Barbuy (1999)
15631.110	3.640	-3.980	Mélendez & Barbuy (1999)
15631.950	5.350	-0.150	Mélendez & Barbuy (1999)
15638.950	5.810	-1.810	Mélendez & Barbuy (1999)
15639.480	6.410	-0.870	Mélendez & Barbuy (1999)
15645.010	6.310	-0.540	Mélendez & Barbuy (1999)
15647.410	6.330	-1.090	Mélendez & Barbuy (1999)
15648.520	5.430	-0.800	Mélendez & Barbuy (1999)
15652.870	6.250	-0.190	Mélendez & Barbuy (1999)
15656.640	5.870	-1.900	Mélendez & Barbuy (1999)
15662.010	5.830	+0.000	Mélendez & Barbuy (1999)
15662.320	6.330	-1.020	Mélendez & Barbuy (1999)
15665.240	5.980	-0.600	Mélendez & Barbuy (1999)
22239.040	5.385	-3.121	Kupka et al. (1999)
22257.097	5.064	-0.723	Kupka et al. (1999)
22260.185	5.086	-0.952	Kupka et al. (1999)
^a 23566.671	6.144	0.306	Kupka et al. (1999)
^a 23572.267	5.874	-0.886	Kupka et al. (1999)
Ni I			
15605.6800	5.300	-0.590	Mélendez & Barbuy (1999)
15605.7500	5.300	-1.010	Mélendez & Barbuy (1999)
15632.6200	5.310	-0.130	Mélendez & Barbuy (1999)

^a Not used for the chemical composition determination.**Table B2.** List of molecular lines selected for calculations together with gf -values and excitation potentials.

Wavelength (air) (Å)	EP (eV)	$\log gf$	Ref.
¹²C¹⁴N			
15594.607	0.9162	-1.645	Kurucz (1999)
15594.610	1.1079	-1.240	Kurucz (1999)
15594.816	1.1770	-1.097	Kurucz (1999)
15595.729	0.9218	-2.106	Kurucz (1999)
15597.719	1.3900	-1.443	Kurucz (1999)
15599.961	1.2391	-1.807	Kurucz (1999)
15605.217	1.2601	-1.810	Kurucz (1999)
15606.718	0.9095	-2.116	Kurucz (1999)
15607.198	1.5181	-1.318	Kurucz (1999)
15609.198	0.9361	-1.479	Kurucz (1999)
15613.554	1.0521	-1.645	Kurucz (1999)
15613.557	1.1770	-1.090	Kurucz (1999)
15615.246	1.0359	-1.645	Kurucz (1999)
15617.057	1.1080	-1.231	Kurucz (1999)
15617.646	1.3900	-1.435	Kurucz (1999)
15622.431	0.9162	-1.637	Kurucz (1999)
15624.806	1.5182	-1.311	Kurucz (1999)
15626.993	0.9345	-2.088	Kurucz (1999)
15629.867	1.2602	-1.798	Kurucz (1999)
15631.866	0.9362	-1.473	Kurucz (1999)
15636.015	0.9218	-2.097	Kurucz (1999)
15636.361	1.2816	-1.801	Kurucz (1999)
15636.584	1.1314	-1.231	Kurucz (1999)
15637.521	0.9357	-1.633	Kurucz (1999)
15640.865	1.4182	-1.436	Kurucz (1999)
15643.764	1.0688	-1.632	Kurucz (1999)
15643.965	1.0521	-1.632	Kurucz (1999)
15646.246	1.2059	-1.090	Kurucz (1999)
15658.785	1.1314	-1.223	Kurucz (1999)
15659.161	0.9476	-2.070	Kurucz (1999)
15660.014	1.5516	-1.313	Kurucz (1999)
15660.688	1.4182	-1.428	Kurucz (1999)
15660.705	1.2817	-1.789	Kurucz (1999)
15661.584	0.9612	-1.471	Kurucz (1999)
15664.879	1.2059	-1.083	Kurucz (1999)
15664.966	0.9358	-1.626	Kurucz (1999)
15666.270	0.9345	-2.079	Kurucz (1999)
22172.254	1.2026	-1.762	Kurucz (1999)
22174.832	1.0475	-3.212	Kurucz (1999)
22186.906	1.0849	-2.206	Kurucz (1999)
22189.293	1.0975	-2.868	Kurucz (1999)
22189.324	1.7232	-2.022	Kurucz (1999)
22190.012	1.0975	-2.273	Kurucz (1999)
22192.684	1.1177	-2.235	Kurucz (1999)
22194.477	1.2309	-1.747	Kurucz (1999)
22196.680	1.4573	-1.875	Kurucz (1999)
22198.914	1.4373	-1.872	Kurucz (1999)
22198.955	1.6007	-1.825	Kurucz (1999)
22216.477	1.2165	-1.747	Kurucz (1999)
22220.176	1.1036	-2.055	Kurucz (1999)
22228.924	1.1079	-2.204	Kurucz (1999)
22228.994	1.3036	-1.633	Kurucz (1999)
22236.898	1.1074	-2.249	Kurucz (1999)
22239.814	1.6007	-1.816	Kurucz (1999)
22243.514	1.2456	-1.732	Kurucz (1999)
22245.525	1.3622	-1.803	Kurucz (1999)
22245.752	1.1285	-2.213	Kurucz (1999)
22248.297	1.4573	-1.862	Kurucz (1999)
22248.438	1.4777	-1.866	Kurucz (1999)
22262.354	1.2309	-1.732	Kurucz (1999)
22273.969	1.6282	-1.818	Kurucz (1999)

Table B2 – continued

Wavelength (air) (Å)	EP (eV)	log <i>gf</i>	Ref.
22276.160	1.3036	-1.624	Kurucz (1999)
22277.008	1.1080	-2.197	Kurucz (1999)
22280.246	1.1036	-2.047	Kurucz (1999)
22285.527	1.1177	-2.225	Kurucz (1999)
22294.160	1.2609	-1.718	Kurucz (1999)
22295.695	1.1216	-2.042	Kurucz (1999)
22296.930	1.3900	-1.803	Kurucz (1999)
22299.426	1.4778	-1.853	Kurucz (1999)
22300.430	1.1397	-2.192	Kurucz (1999)
22301.910	1.4986	-1.856	Kurucz (1999)
22302.410	1.3260	-1.624	Kurucz (1999)
22309.961	1.2457	-1.718	Kurucz (1999)
22311.473	1.2942	-2.377	Kurucz (1999)
22314.611	1.6282	-1.809	Kurucz (1999)
22317.520	1.7561	-2.009	Kurucz (1999)
22321.525	1.1314	-2.195	Kurucz (1999)
¹² C ¹⁶ O			
15590.144	0.4690	-7.3583	Goorvitch (1994)
15591.363	0.1427	-7.7310	Goorvitch (1994)
15592.908	0.4901	-7.3428	Goorvitch (1994)
15594.223	0.1313	-7.7545	Goorvitch (1994)
15595.946	0.5118	-7.3273	Goorvitch (1994)
15597.348	0.1204	-7.7786	Goorvitch (1994)
15599.257	0.5339	-7.3121	Goorvitch (1994)
15600.737	0.1100	-7.8035	Goorvitch (1994)
15602.842	0.5564	-7.2971	Goorvitch (1994)
15604.392	0.1000	-7.8294	Goorvitch (1994)
15606.702	0.5794	-7.2822	Goorvitch (1994)
15608.312	0.0905	-7.8564	Goorvitch (1994)
15612.497	0.0814	-7.8841	Goorvitch (1994)
15615.250	0.6268	-7.2530	Goorvitch (1994)
15616.948	0.0729	-7.9133	Goorvitch (1994)
15619.940	0.6512	-7.2385	Goorvitch (1994)
15621.663	0.0648	-7.9439	Goorvitch (1994)
15624.908	0.6760	-7.2242	Goorvitch (1994)
15626.644	0.0572	-7.9755	Goorvitch (1994)
15630.155	0.7012	-7.2101	Goorvitch (1994)
15631.891	0.0500	-8.0092	Goorvitch (1994)
15635.682	0.7269	-7.1961	Goorvitch (1994)
15637.404	0.0434	-8.0446	Goorvitch (1994)
15641.490	0.7531	-7.1822	Goorvitch (1994)
15643.182	0.0372	-8.0824	Goorvitch (1994)
15647.580	0.7797	-7.1685	Goorvitch (1994)
15649.227	0.0314	-8.1226	Goorvitch (1994)
15653.953	0.8068	-7.1548	Goorvitch (1994)
15655.537	0.0262	-8.1659	Goorvitch (1994)
15660.610	0.8343	-7.1412	Goorvitch (1994)
15662.115	0.0214	-8.2128	Goorvitch (1994)
15667.552	0.8622	-7.1277	Goorvitch (1994)
15668.960	0.0172	-8.2640	Goorvitch (1994)
23550.868	1.2764	-4.9838	Goorvitch (1994)
23550.681	1.4307	-4.2927	Goorvitch (1994)
23552.653	0.8557	-4.5830	Goorvitch (1994)
23553.886	0.2917	-5.4983	Goorvitch (1994)
23554.786	0.0048	-6.4587	Goorvitch (1994)
23556.234	1.4594	-4.2830	Goorvitch (1994)
23558.269	0.8385	-4.5974	Goorvitch (1994)
23562.231	1.4886	-4.2734	Goorvitch (1994)
23564.307	0.8218	-4.6121	Goorvitch (1994)
23564.951	2.1495	-4.3503	Goorvitch (1994)
23568.674	1.5182	-4.2638	Goorvitch (1994)
23569.863	2.5598	-4.7140	Goorvitch (1994)
23570.723	0.2870	-5.5423	Goorvitch (1994)

Table B2 – continued

Wavelength (air) (Å)	EP (eV)	log <i>gf</i>	Ref.
23570.766	0.8056	-4.6271	Goorvitch (1994)
23575.563	1.5482	-4.2545	Goorvitch (1994)
23577.647	0.7898	-4.6424	Goorvitch (1994)
23577.693	0.0071	-6.3642	Goorvitch (1994)
23582.901	1.5786	-4.2451	Goorvitch (1994)
23582.995	2.1902	-4.3426	Goorvitch (1994)
23584.949	0.7744	-4.6582	Goorvitch (1994)
23587.982	0.2827	-5.5907	Goorvitch (1994)
23590.689	1.6095	-4.2359	Goorvitch (1994)
23592.672	0.7596	-4.6743	Goorvitch (1994)
23594.794	2.6067	-4.7071	Goorvitch (1994)
23598.928	1.6408	-4.2268	Goorvitch (1994)
23600.817	0.7451	-4.6908	Goorvitch (1994)
23601.032	0.0100	-6.2876	Goorvitch (1994)
23601.535	2.2314	-4.3350	Goorvitch (1994)
23605.665	0.2789	-5.6445	Goorvitch (1994)
23607.621	1.6725	-4.2177	Goorvitch (1994)
23609.383	0.7312	-4.7077	Goorvitch (1994)
23616.77	1.7047	-4.2088	Goorvitch (1994)
23618.369	0.7177	-4.7251	Goorvitch (1994)
23620.259	2.6541	-4.7001	Goorvitch (1994)
23620.571	2.2729	-4.3273	Goorvitch (1994)
23623.771	0.2756	-5.7051	Goorvitch (1994)
23624.802	0.0133	-6.2232	Goorvitch (1994)
23626.375	1.7373	-4.2000	Goorvitch (1994)
23627.778	0.7046	-4.7430	Goorvitch (1994)
23636.44	1.7703	-4.1912	Goorvitch (1994)
23637.608	0.6921	-4.7617	Goorvitch (1994)
23640.108	2.3148	-4.3198	Goorvitch (1994)
23642.301	0.2728	-5.7747	Goorvitch (1994)
¹² C ¹⁷ O			
23555.604	0.5678	-4.9176	Goorvitch (1994)
23558.862	0.0255	-5.9974	Goorvitch (1994)
23561.873	0.5513	-4.9326	Goorvitch (1994)
23568.546	0.5353	-4.9473	Goorvitch (1994)
23575.626	0.5198	-4.9630	Goorvitch (1994)
23583.110	0.5047	-4.9788	Goorvitch (1994)
23591.000	0.4901	-4.9948	Goorvitch (1994)
23599.294	0.4759	-5.0114	Goorvitch (1994)
23607.995	0.4621	-5.0284	Goorvitch (1994)
23617.100	0.4489	-5.0459	Goorvitch (1994)
23626.613	0.4360	-5.0639	Goorvitch (1994)
23636.530	0.4237	-5.0825	Goorvitch (1994)
¹² C ¹⁸ O			
23556.518	0.2538	-5.4594	Goorvitch (1994)
23564.155	0.2389	-5.4752	Goorvitch (1994)
23572.184	0.2245	-5.4913	Goorvitch (1994)
23580.602	0.2105	-5.5079	Goorvitch (1994)
23589.412	0.1970	-5.5251	Goorvitch (1994)
23598.614	0.1839	-5.5426	Goorvitch (1994)
23608.206	0.1712	-5.5607	Goorvitch (1994)
23618.19	0.1590	-5.5792	Goorvitch (1994)
23628.565	0.1473	-5.5984	Goorvitch (1994)
23639.333	0.1360	-5.6182	Goorvitch (1994)
¹³ C ¹⁶ O			
23560.596	1.3099	-4.9751	Goorvitch (1994)
23563.521	0.1719	-5.5580	Goorvitch (1994)
23570.753	1.3437	-4.9666	Goorvitch (1994)
23573.485	0.1596	-5.5766	Goorvitch (1994)
23581.341	1.3779	-4.9582	Goorvitch (1994)
23583.842	0.1478	-5.5957	Goorvitch (1994)
23592.363	1.4126	-4.9496	Goorvitch (1994)
23594.59	0.1365	-5.6156	Goorvitch (1994)

Table B2 – *continued*

Wavelength (air) (Å)	<i>EP</i> (eV)	$\log gf$	Ref.
23603.818	1.4476	-4.9412	Goorvitch (1994)
23605.733	0.1256	-5.6360	Goorvitch (1994)
23615.711	1.4831	-4.9329	Goorvitch (1994)
23617.268	0.1151	-5.6574	Goorvitch (1994)
23628.043	1.5189	-4.9248	Goorvitch (1994)
23629.197	0.1051	-5.6794	Goorvitch (1994)
23640.814	1.5552	-4.9165	Goorvitch (1994)
23641.522	0.0956	-5.7025	Goorvitch (1994)
OH			
15593.179	0.8740	-5.358	Kurucz (1999)
15593.563	0.8740	-5.358	Kurucz (1999)
15608.357	0.4942	-7.209	Kurucz (1999)
15609.683	0.4942	-7.209	Kurucz (1999)
15621.766	0.8374	-6.734	Kurucz (1999)
15624.434	0.8415	-7.006	Kurucz (1999)
15624.660	0.1336	-8.233	Kurucz (1999)
15626.704	0.5413	-5.198	Kurucz (1999)
15627.290	0.8871	-5.435	Kurucz (1999)
15627.293	0.8871	-5.435	Kurucz (1999)
15627.413	0.5413	-5.198	Kurucz (1999)
15628.902	0.1337	-8.233	Kurucz (1999)
15636.235	0.8876	-7.202	Kurucz (1999)
15636.596	0.8876	-7.202	Kurucz (1999)
15643.302	0.8420	-7.007	Kurucz (1999)
15650.557	0.8643	-5.587	Kurucz (1999)
15650.797	0.8643	-5.587	Kurucz (1999)
15651.896	0.5341	-5.132	Kurucz (1999)
15653.480	0.5343	-5.132	Kurucz (1999)
15654.116	0.8383	-6.734	Kurucz (1999)
15655.053	0.3041	-7.713	Kurucz (1999)
15658.127	0.3038	-7.713	Kurucz (1999)